ELSEVIER

Nuclear Instruments and Methods in Physics Research A 491 (2002) 194–215

NUCLEAR INSTRUMENTS & METHODS IN PHYSICS RESEARCH Section A

www.elsevier.com/locate/nima

Simulation of non-ionising energy loss and defect formation in silicon

M. Huhtinen*

CERN, CH-1211 Geneva 23, Switzerland

Received 4 October 2001; received in revised form 25 April 2002; accepted 27 May 2002

Abstract

Simulation studies of Non-Ionising Energy Loss (NIEL) in silicon exposed to various types of hadron irradiation are presented. A simulation model of migration and clustering of the produced primary defects is developed. Although there are many uncertainties in the input parameters it is shown that the model is consistent with experimental observations on standard and oxygen-enriched silicon. However, the model makes the rather dramatic prediction that NIEL scaling of leakage current and effective doping concentration can be violated significantly even in standard silicon. Although there are possible shortcomings in the model which might account for this, it is shown that at the microscopic level there is, indeed, no obvious reason for an exact NIEL scaling. Furthermore, it is argued that, contrary to common belief, even a significant violation of NIEL scaling can still be consistent with experimental data.

PACS: 61.80.Az; 61.80.Hg; 61.82.Fk

Keywords: NIEL; Defect cluster; Silicon radiation damage

1. Introduction

Silicon bulk damage, which will be the limiting factor of detector lifetime at the LHC experiments, has been studied for several decades. The Non-Ionising Energy Loss (NIEL) scaling hypothesis of bulk damage, i.e. the claim that changes of electrical properties are proportional to NIEL, has become generally accepted because it has agreed with most experimental data for various irradiation conditions [1]. For pioneering work on NIEL see Refs. [2–7] and for a recent review [8] and references therein. NIEL scaling has been used as the basis of almost all damage predictions, and it has sometimes even been applied to determine irradiation fluences or spectra. Due to its success, the validity of NIEL scaling has been rarely questioned.

However, there is still no microscopic understanding of why damage should scale with NIEL. Actually, there have so far been no tools to reliably calculate NIEL from first principles for high-energy hadrons. The work in Ref. [9] is sometimes quoted as a NIEL calculation for protons and used as a justification that NIEL scaling is valid between high-energy protons and 1 MeV neutrons. Apparently, it is often overlooked that the proton

*Tel.: +41-22-767-1579; fax: +41-22-767-8940.
E-mail address: mika.huhtinen@cern.ch (M. Huhtinen).

0168-9002/02/$ - see front matter
PII: S0168-9002(02)01227-5

NIEL curve given in Ref. [9] is obtained from a fit to experimental damage data and from this the pion damage is extrapolated under the assumption that NIEL scaling would be valid. The agreement of experimental pion data [10,11] and the predictions in Ref. [9] suggests that NIEL scaling cannot be badly violated between protons and pions, but the proton NIEL quoted in that work is by no means a theoretical prediction.

During the last few years the ROSE collaboration, studying defect engineering of silicon, has published convincing data which clearly are in contradiction with the NIEL hypothesis in some special cases [8]. These data have cast first doubts on the validity of the NIEL hypothesis in general. The main aim of this study is to present a fully microscopic simulation of NIEL in silicon in order to contribute to a deeper understanding of the NIEL scaling and in particular the possible role of oxygen in the silicon.

2. Simulation model

The simulations proceed in several steps. The first half of this paper deals with the generation of hadronic interactions and the transport of the produced heavy recoils which initiate a full atomic cascade. This first part of the simulations provides a fully microscopic prediction of NIEL for various particle types and energies.

The second phase of the simulations considers the vacancies and interstitials formed by the atomic cascade. These are assumed to undergo a random walk with recombination probabilities extracted from Deep Level Transient Spectroscopy (DLTS) data of irradiated silicon. This part of the simulations is aimed at understanding qualitatively the formation of stable defects. It should be emphasised that the models used are not really microscopic in the same sense as molecular dynamics simulations, where proper potentials are used to describe the interactions between defects. In the model employed here it is assumes that the interactions between various defect types—be they due to electrical charges or lattice strain—are implicitly included by fitting the model to experimental DLTS data. This fitting procedure also means that the results correspond to the instant of time when the DLTS data has been taken, i.e. any annealing which has taken place at the time of the DLTS measurement is implicitly included in the model. The probably most severe deficiency caused by not explicitly modelling the interactions is that no difference can be made between cluster regions where the crystalline structure is severely distorted and the surrounding, mostly undistorted, silicon.

Finally, the stable defects are analysed in terms of their electrical properties to predict leakage current (I_{leak}) increase and changes of effective doping concentration (N_{eff}). Several rather vague assumptions of the electrical behaviour of defects, which had to be introduced at this stage, will be discussed later in this paper.

Despite a fairly large number of uncertain assumptions and approximations, the model should provide some insight into the defect formation in silicon and, in particular, the effects of oxygen. It must be emphasised, however, that—contrary to the NIEL predictions—the defect formation part of these simulations does not really intend to be predictive at a quantitative level. The goal is merely to show that the experimental findings of the ROSE collaboration can be consistent with a model based on reasonable assumptions. Nevertheless, it will be seen that the model makes interesting qualitative predictions for NIEL scaling of I_{leak} and N_{eff}.

2.1. Hadronic interactions

As described in Ref. [12], three different simulation codes are needed for the generation of all hadronic interactions of interest. Most complicated is the generation of inelastic hadronic interactions because a multitude of reaction channels are possible. Consequently the simulation of these reactions includes the largest uncertainties. At hadron energies below 1.3 GeV a pre-equilibrium model is used [13]. Above 5 GeV/c the high-energy hadronic module of the FLUKA [14] code is invoked. The energy gap is bridged by a resonance production and decay model [15]. While the pre-equilibrium model can be expected to provide a fairly reliable fragment distribution,

much less attention has been paid to fragment yields at the higher energies. In a previous paper [12] utilising these same event generators good results were obtained for predicting Single Event Upsets (SEU) at energies up to 200 MeV. More recently, a similar study [16] was compared with 120 GeV pion beam-test data and good agreement was observed [17]. Although these result give confidence in the fragment spectra, it should be pointed out that, compared to a NIEL simulation, SEU studies are much more sensitive to having correct fragment charge and energy distributions because SEU rates are determined by the maximum charge and energy the fragments can have. NIEL, however, represents only a small fraction of the energy loss of recoils and becomes important only at the end of the range of an ion. In fact, an Si-recoil will deposit roughly the same NIEL—slightly below 300 keV in silicon—no matter how high its initial energy, provided it exceeds about 3 MeV.

A second model is needed for the simulation of elastic hadron-Si scattering. For this purpose a rather simple Glauber optical model is used [18,19]. This has the drawback that it tends to overestimate scattering to large angles—an effect which can become significant especially at high energies. To avoid unphysically high values a maximum of 10 MeV is imposed on the recoil from elastic scattering. Although this cut is completely arbitrary, it has no effect on the results because NIEL saturates above 3 MeV. Even with this cut the cross-section for large angle scattering remains overestimated. But since the elastic cross-section decreases very rapidly with increasing angle the effect on the average NIEL is negligible.

Neutron interactions at energies below 20 MeV are generated by direct sampling from ENDF/B-VI data.

Detailed recoil energy spectra provided by these models and a discussion of their reliability can be found in Ref. [12].

2.2. Transport of recoil ions

The produced recoil ions are transported with a modified version of the TRIM code [20]. Ion energy losses and mean ranges are given in Ref. [12]. All ion species, including protons, are transported.

During the transport the energy loss is recorded in detail. Because NIEL becomes important only at low ion energies special emphasis has been paid to this part by continuing the detailed TRIM simulation down to the displacement threshold E_D. The value of E_D is not exactly known, thus it is the first parameter in the model which can be tuned to some extent—the lower the value of E_D, the more vacancies and interstitials will be created. Of course, all recoils from atomic scattering, provided their energy exceeds E_D, have to be explicitly transported also. The transport stops when all recoils in the atomic cascade have energies below E_D or have escaped the silicon, which is assumed to be 300 μm thick and infinitely wide. At the end of the TRIM transport a large number of vacancies (V) and Si interstitials (I) have been generated and for all of them exact positions are known.

2.3. Migration and combination of defects

The last step of the procedure is to simulate the migration of the defects. Several defect kinetics models have been proposed [21–23]. In the model proposed in Ref. [21], the defects migrate through the lattice and combine with each other or with impurities. Since an initially uniform distribution of defects is assumed and because all defects will ultimately be captured somewhere, this model does not need the absolute value of a capture radius or probability. The relative formation rate of a complex defect XY is given by

$$\frac{P(X,Y)[Y]}{\sum_i P(X,Z_i)[Z_i]} \tag{1}$$

where $P(X,Y)$ is the probability[1] for reaction $X+Y\rightarrow XY$, $[Y]$ is the concentration of Y and Z_i is any defect or impurity (including Y) which could capture X.

However, the defect distribution resulting from the TRIM transport is explicitly non-uniform and the purpose of the present study is to understand

[1] The original paper [21] uses the term capture radius for what is actually a capture probability.

the consequences of this non-uniformity. In this case, the absolute value of the capture radius is needed, because it controls the opacity of the initially very dense defect cluster. If the capture probability is low the defects are relatively free to escape and the clusters will dilute to a large extent. On the contrary, if the capture probability is high there will be more immediate combinations within the cluster itself. In the latter case, I + V reactions will reduce the number of defects and V + V reactions will increase the number of closely packed V_2 defects.

Most of the defect kinetics models have to treat the V_2 as a primary defect. The reason for this is that when a spatially uniform Frenkel pair (I + V) generation is assumed, the encounter and combination of two vacancies would be an extremely rare event. A reasonable assumption for the capture time of a vacancy on an impurity is about 1 s in normal silicon at room temperature and much less in oxygen-enriched Si [21]. Typically, irradiations are done at fluxes well below 10^{10} cm^{-2} s^{-1}. Assuming this flux and a cross-section of about 4000 mb (1 MeV neutrons in Si) there will be about 2×10^9 cm^{-3} s^{-1} atomic cascades produced—each with an average of 350 vacancies. Thus, the uniformised density of vacancies produced within the average vacancy lifetime remains below 10^{12} cm^{-3}. In addition, the clustering introduces significant density fluctuations and more than 90% of vacancies annihilate in I + V reactions already within the cluster (according to Ref. [5] and this work). Thus, encounters of vacancies from different events are very rare. Actually, if this would not be the case, it should become visible as a clear rate dependence in bulk damage tests.

In reality the V_2 is not a primary defect but must result from V + V reactions within the dense clusters produced by hadronic collisions.[2] The TRIM simulation produces only vacancies and interstitials but since it also reproduces the density variations due to clustering, the V_2 introduction rate, as well as that of any other complex defect, should result from reactions between these two primary defects—and possible pre-existing impurities.

It would be too complicated to analyse the variations of the local defect density within a cluster in order to use simple diffusion equations during the defect migration. Instead a straightforward Monte-Carlo method is applied by treating each defect as a random walker which jumps from one lattice site to the next. However, even though several biasing tricks can be applied, it is very CPU consuming to transport those defects which have managed to escape the cluster region. Therefore, a somewhat arbitrary criterium has been used to determine when the defect has migrated out of the cluster. This is assumed to have happened when it is farther than 1000 Å from its original site and there are no other defects within 200 Å. Such escaped defects are assumed to be uniformly distributed in the material and are treated according to the model described in Ref. [21] assuming uniform distribution of all previously generated defects. During defect migration the silicon is assumed infinite, i.e. possible effects at crystal boundaries are not taken into account.

After each random walk step the surroundings of the defect are checked and if another defect is found within a predefined capture radius (R_0) a possible combination of the defects is considered. The decision if two defects combine is based on the capture probabilities, as given in Table 1. The value of R_0 is set to 16.2 Å, corresponding to 3 lattice constants. This value is selected such that it is larger than any of the capture radii (R) in Table 1. This is required in order to keep the probability of capture, $P = (R/R_0)^3$, below unity. The TRIM phase does not take into account the discrete lattice structure, but vacancies and interstitials are distributed continuously and independent of each other. Due to the probabilistic nature of the recombination, with R_0 much larger than a lattice spacing, this is of no concern.

Initially—before any stepping is done—the constellation of vacancies and interstitials is checked and prompt recombinations are allowed. For this initial step a list of nearest neighbours is established for each defect and the sampling of

[2] V_2 production is observed also in electron irradiation, where no clusters are formed. However, even in this case 'mini-clusters' consisting of a few nearby vacancies are created which are enough to account for formation of some di-vacancies.

Table 1
List of reactions and their capture radii. The V + V value is taken from MD simulations and fixes the absolute scale of the whole set. The values followed by (fit) are fitted to DLTS data. The values in parentheses are based on assumptions described in the text. All other values are taken from Refs. [21,24]. The probabilities are with respect to the predefined 16.2 Å radius.

Reaction	R (Å)	Probability	Reaction	R (Å)	Probability
$V + I \rightarrow Si$	16.0 (fit)	0.956	$I + I \rightarrow I_2$	7.9 (fit)	0.118
$V + V \rightarrow V_2$	7.7 (MD)	0.107	$I + V_2 \rightarrow V$	15.8 (fit)	0.934
$V + V_2 \rightarrow V_3$	9.9 (fit)	0.226	$I + V_3 \rightarrow V_2$	(12.4)	0.445
$V + O \rightarrow VO$	5.0	0.029	$I + VO \rightarrow O$	8.6	0.149
$V + VO \rightarrow V_2O$	8.4	0.139	$I + V_2O \rightarrow VO$	(5.1)	0.031
$V + V_2O \rightarrow V_3O$	5.7	0.043	$I + V_3O \rightarrow V_2O$	(11.7)	0.374
$V + P \rightarrow VP$	12.2	0.429	$I + VP \rightarrow P$	7.4	0.093
$V + I_2 \rightarrow I$	(15.3)	0.849	$I + C_s \rightarrow C_i$	7.4	0.093
$V + ICC \rightarrow CC$	(8.6)	0.149	$I + CC \rightarrow ICC$	14.2	0.673
$V + ICO \rightarrow CO$	(10.8)	0.298	$I + CO \rightarrow ICO$	11.3	0.336

possible recombination is done in increasing order of distance. During the defect migration the maintaining of such a list would be too CPU consuming and in this case the recombination with defects falling within the capture radius is sampled randomly.

The capture radii given in Ref. [24] are obtained from defect concentrations after electron irradiation where correlations between certain defects are likely to be different than in hadron irradiated material. For instance, the relative probabilities of V + O and V + V should be influenced by the fact that vacancies are generated in clusters while oxygen is a uniformly distributed impurity. For reactions with impurities, e.g. V + O and V + P, the relative probabilities should not depend on the type of irradiation. All capture radii, which in Ref. [24] are given with respect to V + V, can be translated to be relative to V + O so that the only uncertainty remaining is, if the ratio between V + O and V + V depends on the type of irradiation. A variation of this ratio showed that results are not very sensitive to it. This is probably because V + V take place within a cluster and V + O mostly outside, so the ratio between VO and V_2 is determined by the fraction of vacancies escaping the cluster, not the relative probability between V + V and V + O. Another potentially important uncertainty arising from the use of electron data is the formation of higher-order multi-vacancies, in particular V_3. For the $V + V_2$ reaction a capture radius was quoted in Ref. [24], but this value might be significantly higher inside a dense cluster. Therefore, this value has not been used but the $V + V_2$ probability has been re-fitted using the defect assignment proposed in Ref. [25] and DLTS data given in Ref. [27].

The relative capture radii given in Ref. [24] do not provide all the data needed for the present simulation. The two most important missing probabilities are those for I + V and $I + V_2$. In addition, an absolute scale for the capture radii is needed because it controls the transparency of cluster regions.

Molecular dynamics (MD) simulations [26] suggest that the capture radius for V + V would be about 7.7 Å, which is used to set the absolute scale. A variation of this value revealed that results are not very sensitive to it, because the other free parameters are able to adjust themselves to some extent.

An analysis of available DLTS data of neutron irradiated silicon gives four independent relations, which can be expressed as introduction rates of defects [27,28]:

$$\frac{[V_2]}{[VO]} \approx 1.5$$

$$\frac{[VO] + 2 \times [V_2]}{[CC] + [CO]} \approx 1.7,$$

$$\text{Introduction rate of VO } ([VO]) \approx 0.7\ \text{cm}^{-1},$$

$$\text{Introduction rate of } V_3\ ([V_3]) \approx 0.5\ \text{cm}^{-1}. \quad (2)$$

Since it can be assumed that both CC and CO are preceded by a $I + C_s \rightarrow C_i$ reaction, the second expression is essentially the ratio of all detected vacancies and interstitials. The value different from unity is clearly inconsistent with the set of defects presented in Ref. [24], indicating that there must be an additional reaction which causes interstitials to disappear into invisible defects. It has been suggested [23,29] that this could be interstitial clustering, $I + I \rightarrow I_2$. Such defects have not been observed so there is no firm evidence, but this reaction can also be considered as any generic sink for interstitials. With this new reaction there are in total four free parameters to be fitted using the four constraints of Eq. (2). A summary of reactions, capture radii and reaction probabilities is given in Table 1. As stated before, this fitting procedure is assumed to implicitly account for all interactions between various defects and impurities.

Some of the reaction probabilities in Table 1 could not be found in literature and there were not enough constraints from DLTS data to fit them. These were obtained—rather arbitrarily—from known probabilities by a kind of inverse reaction consideration. For instance, the probability for $I + V_2O$ was obtained from

$$P(I, V_2O) = P(I, VO) \times \frac{P(V, O)}{P(V, VO)}. \quad (3)$$

According to MD simulations [30] the formation energy of $V + V_n$ is of similar magnitude up to $n = 5$. Motivated by this multi-vacancies were generated up to V_6 with the capture probability $P(V, V_n)$ for $n > 2$ set equal to $P(V, V_2)$. Correspondingly $P(I, V_n)$ for $n > 3$ was set equal to $P(I, V_3)$. Although these methods are at best very approximate, the defects concerned are expected to have little impact on the final result and are included mainly for the sake of completeness.[3]

In the set of reactions listed in Table 1, those involving carbon are a special case because carbon interstitials migrate very slowly in the lattice. Whereas all other reactions involving V and I can be assumed to take place within a second, carbon interstitials can move for days in the lattice before forming CC or CO. Thus, the dynamics of the system depends on the irradiation rate, which introduces a severe complication into the simulations. Two limiting cases, however, are rate independent:

(1) Fast irradiation (or low temperature). In this case, no ICC and ICO will be formed because all interstitials have disappeared before CC or CO have been created.
(2) Slow irradiation (or high temperature). In this case, there are no free C_i and CC, CO, ICC and ICO are formed with equilibrium rates.

While the second case is closer to LHC conditions, the first one is likely to be a better representation of typical test conditions where irradiations are usually performed at high fluxes and often with detectors cooled. Thus, in the simulations, it is assumed that neither CC nor CO are formed and only the amount of C_s is reduced by the irradiation. The net effect of this assumption is that, due to suppression of CCI and COI formation, more interstitials are available to annihilate vacancies which leads to a slight reduction of all vacancy related defects. At an initial carbon concentration of 10^{16} cm^{-3}—assumed in all the simulations—the difference between the two assumptions is rather minor because the C_s concentration is remaining larger than that of any radiation-induced defect up to the maximum fluences considered. The effects of different carbon concentrations have not been studied in this work, but from the reaction list in Table 1 it can be seen that carbon atoms are an important sink for interstitials, which otherwise would mostly end up annihilating vacancies. Since vacancy-related defects are suspected to be the main causes of stable damage, a decrease of carbon concentration should increase the radiation hardness of silicon.

3. Results

3.1. NIEL and vacancy generation

When an ion collides with a lattice atom a minimum energy—assumed to be $E_D = 20$ eV in

[3] Various different assumptions were tested for these probabilities and the influence on final results was negligible.

this study—is needed to dislodge the atom from its site. If the energy is lower, the energy transferred will be dissipated by phonons and no damage is created. If the energy transfer is sufficiently high, the kinetic energy of the recoil will be the difference between the energy transfer and the energy E_D wasted into dislodging the atom. Each recoil can dislodge further atoms and is therefore a member on an atomic cascade. If the energy of an ion falls below 20 eV it will not generate any further damage and its remaining energy is dissipated as phonons.

The atomic cascade distributes the total NIEL between collisions with low-energy transfer (phonon excitation) and displacement of lattice atoms. Only the latter part of NIEL is related to damage. For a known displacement threshold E_D the modified Kinchin–Pease [20] relation

$$\begin{aligned} &\nu = 1 \quad \text{if } E_D < E_v < 2.5E_D, \\ &\nu = \frac{E_v}{2.5E_D} \quad \text{if } E_v > 2.5E_D \end{aligned} \tag{4}$$

could be used to get an estimate of the number of displacements ν as a function of the estimated NIEL (E_v) of the recoil. In this work, the TRIM simulation down to E_D replaces the use of Eq. (4)—and provides also full spatial information about initial vacancy distributions. As long as the initial Primary Knock-on Atom (PKA) has an energy much larger than E_D it is reasonable to assume that the partition of NIEL into phonons and damage is independent of the PKA energy. The comparison in Table 2 shows that for 1 MeV neutrons and 24 GeV/c protons slightly less than half of the NIEL goes into damage. For 10 MeV protons, where collisions with low-energy transfer are relatively more important, the fractions are equal. Part of this difference is explained by the fact that the Coulomb cross-section of the initial p-Si collisions was limited to energy transfers above E_D. Thus, the phonon part (and the total NIEL) is somewhat underestimated. Table 2 allows to conclude that with good accuracy the number of hadron induced displacements is proportional to the total NIEL. It should be also noted that the values listed in Table 2 are in excellent agreement with the 40% damage fraction predicted by Eq. (4).

Table 2
Partition of NIEL (MeV mb) into phonons and displacements for different hadron projectiles

	10 MeV Proton	24 GeV/c Proton	1 MeV Neutron
σ (MeV mb)	292	47.2	76.9
Phonons	147	27.2	44.1
Displacements	145	20.0	32.8
Displace./total (%)	50	42	43

Fig. 1 shows the simulated NIEL cross-section[4] as a function of particle energy for protons, positive pions and neutrons above 20 MeV.

Fig. 2 shows a comparison of the proton NIEL simulated in this work with a previous simulation [31]. The dashed line in Fig. 2 shows the effect if experimental elastic scattering data is used instead of the Glauber model between 30 and 95 MeV, as was done in Ref. [9]. A comparison of the two sets of experimental data [4,32] reveals a larger discrepancy than what is observed between the different simulation results. The discrepancy of the data might be related to uncertainties[5] in the neutron NIEL used to normalise the data in Ref. [4]. It will be shown later in this paper that the differences between the I_{leak} and N_{eff} data of Ref. [32] are of central importance for the interpretation of the complete simulation results. The differences between the simulated NIEL at lowest proton energies might be partly explained by the value of the displacement threshold, assumed here to be $E_D = 20$ eV. Since no primary elastic collisions were generated below E_D a lower threshold would result in a higher NIEL at low proton energies, where small angle Coulomb scattering dominates. At higher energies the exact

[4] A NIEL cross-section is the primary hadron-Si cross section times the average NIEL per event. In this paper 'NIEL' will be used as a shorthand for both. The meaning should be obvious from the context.

[5] The ratio of 6.7, quoted in Ref. [4] as the relative damage between the used fission spectrum and 1 MeV neutrons, appears very high but the paper is not clear on the exact scaling procedure.

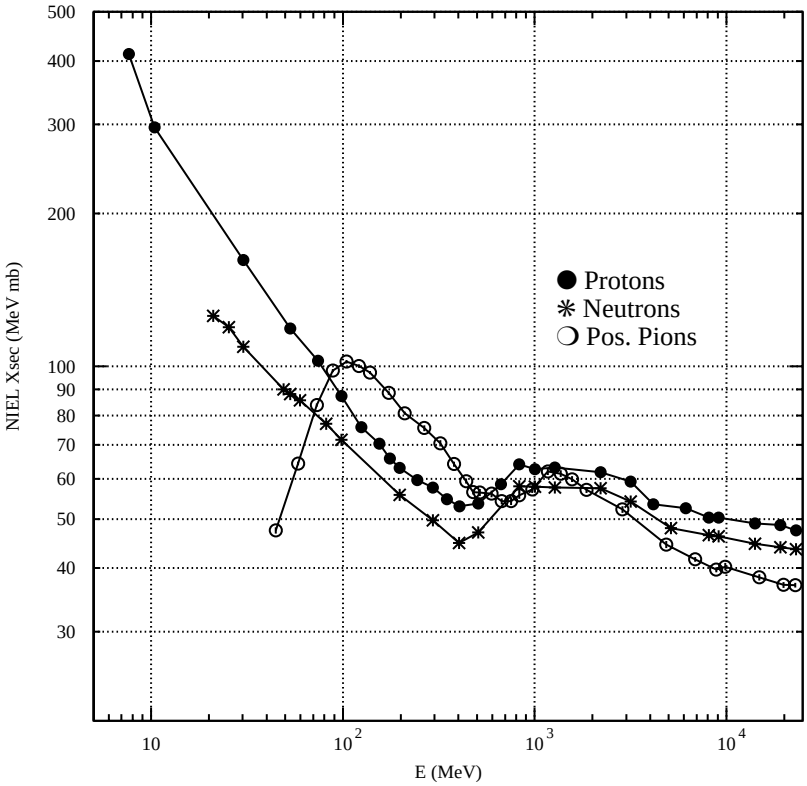

Fig. 1. Simulated NIEL for positive pions, protons and high-energy neutrons. The curves show total NIEL of which about half produces damage (see Table 2). Statistical errors are negligible.

value of this threshold has less influence on the predicted NIEL.

For pions the maximum of NIEL appears at lower energies than previously predicted. It is known, however, that the optical model used in Ref. [9] puts the maximum of the (π, Si) cross-section at a slightly too high energy. Neither the prediction of Fig. 1 nor that in Ref. [9] are inconsistent with experimental data [10,11] where the uncertainties between 100 and 200 MeV are sufficiently large to cover both predictions.

At energies below 20 MeV the neutron NIEL, shown of Fig. 3, has been simulated only at the indicated points. Between these points the shape of the total (n,Si) cross-section from ENDF/B-VI has been used to interpolate.

The neutron NIEL obtained in these simulations is somewhat lower than the values recommended by the ROSE collaboration [1], which are based on Refs. [9,33,34]. Again—at low energies—the most likely explanation is a different value of the displacement threshold or a different treatment of collisions below that threshold. At neutron energies beyond 20 MeV the major uncertainties are likely to be related to the (n, α) cross-section in FLUKA, which has been discussed in Ref. [12]. The magnitude of these uncertainties is reflected in the rather small discontinuity at 20 MeV, where the model changes. However, it is possible that this effect increases towards higher energies as suggested by a comparison of the two curves. No experimental data are known to the author, which would allow to decide which of the two NIEL predictions between 20 MeV and 1 GeV of neutron energy is more correct.

The NIEL given in Table 2 for 1 MeV neutrons differs from 95 MeV mb, which is the defined value of NIEL for 1 MeV neutrons [35,36]. This is due to

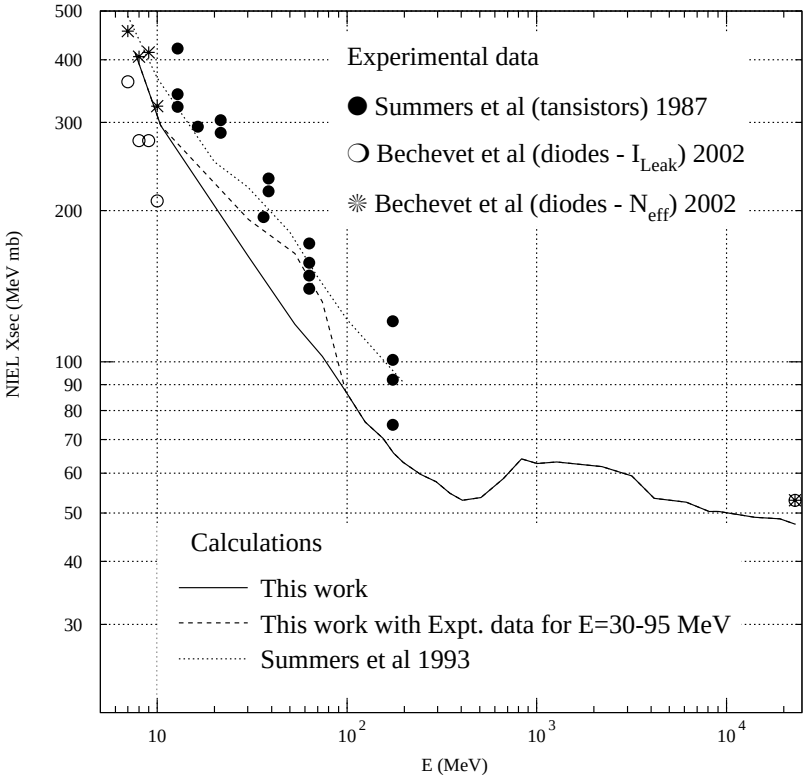

Fig. 2. Simulated NIEL for protons compared with experimental data and other simulations—see text for details and references.

the fact that the simulations were done at exactly 1 MeV whereas the 95 MeV mb are an average over the rapidly varying cross-section in the vicinity of 1 MeV [36]. In the following all results—including those for 1 MeV neutrons—will be renormalised to 95 MeV mb.

For completeness it should be pointed out that, although neutron NIEL is often—including Fig. 3—quoted only above 100 keV, also thermal neutrons can contribute to NIEL. At very low energy a neutron can get captured by a nucleus which subsequently recoils against an emitted gamma ray. However, the cross-sections and recoil energies for thermal neutron-Si scattering are rather small. Presumably, a more significant special case is due to the presence of boron dopants. Upon neutron capture the ^{10}B isotope decays predominantly into an α-particle and a ^{7}Li nucleus. The cross-section is large, and depending on the boron concentration, this reaction can have a non-negligible impact on NIEL. These thermal neutron effects are a somewhat exotic case, which will not be further considered in this study.

The spatial distribution of vacancies varies significantly from one event to the other. One example is shown in Fig. 4, where a single silicon PKA with an energy typical of 1 MeV neutron scattering has been simulated. A characteristic tree-like structure with several sub-clusters can be observed. These sub-clusters correspond to lower energy ions knocked-off from their lattice sites. If the PKA energy is increased above 50 keV a larger tree with several branches—each resembling that of Fig. 4—will be observed.

Fig. 5 shows initial vacancy distributions obtained from the simulations for 10 MeV and 24 GeV/c protons and 1 MeV neutrons. The plots represent a projection over 1 μm in depth for a hadron fluence of 10^{14} cm^{-2}. It can be clearly seen that neutrons tend to produce isolated dense

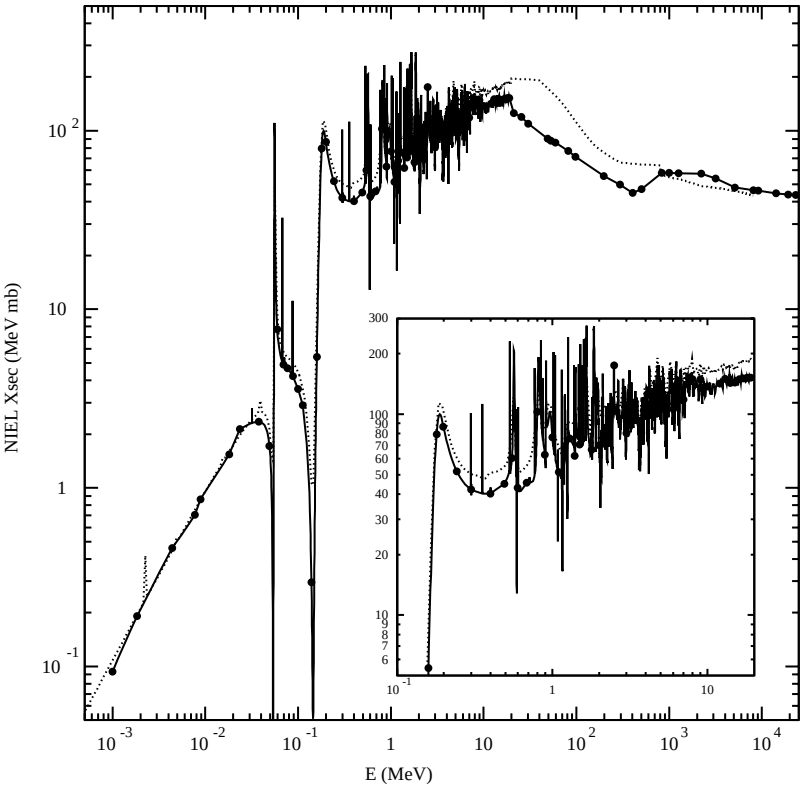

Fig. 3. Simulated NIEL for neutrons. The curves show total NIEL of which about half produces damage (see Table 2). The insert shows an enlargement of the resonance region. The dotted line shows the neutron NIEL recommended by the ROSE collaboration [1].

clusters of vacancies with very few point defects while 10 MeV protons produce a fairly uniform distribution of defects with only a few clusters corresponding to collisions with high momentum transfer. The 24 GeV/c protons form an intermediate case between these two. For the forthcoming discussion, however, it is important to note that all considered radiation types produce vacancy clusters and that in all cases these clusters are far from each other and thus correlations between clusters from different events are very unlikely at fluences below 10^{15} cm^{-2}.

An important parameter is the distribution of vacancy–vacancy distances in each individual event. If vacancies are densely clustered such a distribution should peak at rather low values. If, however, fast recoils or fragments distribute NIEL over longer distances the V–V distance distribution should appear flatter. Indeed, this is what can be observed in Fig. 6. The most probable V–V distance produced by 1 MeV neutron interactions is about 100 Å. A comparison with Fig. 4 shows that this is slightly shorter than typical cluster dimensions. For 24 GeV protons a tail to very large V–V separations is visible, which indicates that part of the NIEL is distributed far outside of cluster regions. The same can be observed for 10 MeV protons, but here the tail is shorter because the maximum recoil energy is limited. It should also be noted that Fig. 6 does not reflect the number of real point defects, i.e. events leading to formation of a single vacancy. For Coulomb scattering about half of the events correspond to such cases. But since these represent only a small fraction of total NIEL, they should not play any important role.

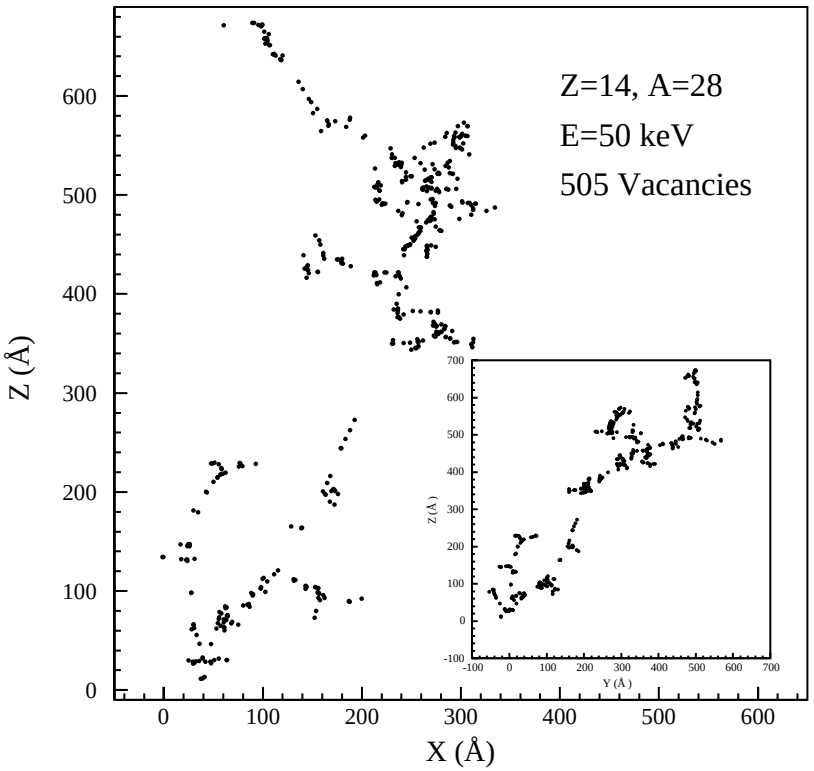

Fig. 4. Spatial distribution of vacancies created by a 50 keV Si-ion in silicon. The inset shows the transverse projection of the same event.

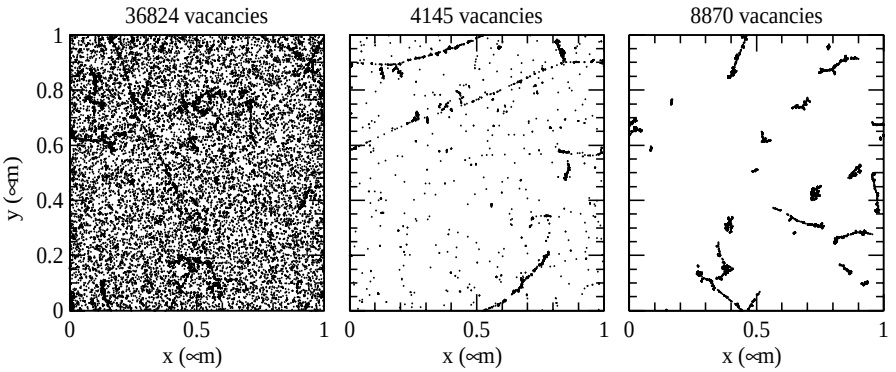

Fig. 5. Initial distribution of vacancies produced by 10 MeV protons (left), 24 GeV/c protons (middle) and 1 MeV neutrons (right). The plots are projections over 1 μm of depth (z) and correspond to a fluence of 10^{14} cm^{-2}.

3.2. Defect formation

Fig. 7 shows a qualitative example of a final constellation of di- and tri-vacancies. The total numbers of the defects indicated in the plot should not be compared with any NIEL scaling because the statistical fluctuations are overwhelmingly large. Also the depth of the projections should be

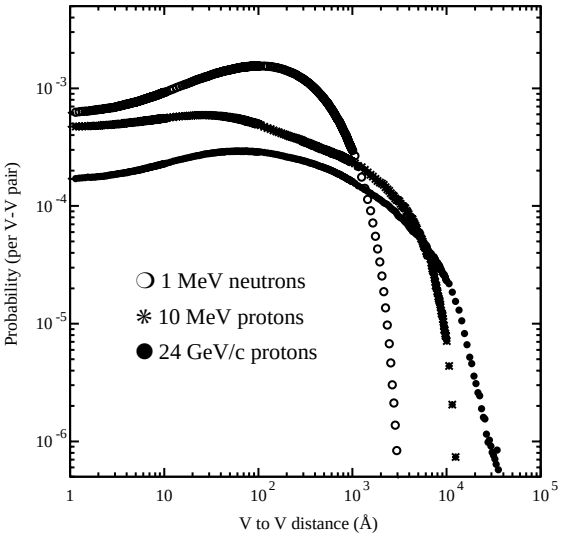

Fig. 6. Probability distribution of vacancy–vacancy distances within a single event. The plot represents an average over many thousand events.

taken into account, i.e. not all defects which appear to be close together are so in reality.

Table 3 shows the fraction of initially produced vacancies ending up in various types of defects. These fractions do not sum up to unity because most of the vacancies are annihilated in an I + V process.

Fig. 8 shows the average density of the most influential defects as a function of fluence for various irradiation types and two values of the oxygen concentration. The simulated NIEL values given in Table 2 have been used to scale all plots to 95 MeV mb.

3.2.1. V_2 formation

Up to a fluence of few times 10^{14} cm^{-2} the evolution of $[V_2]$[6] shows no dependence on [O] and exhibits perfect NIEL scaling.

A comparison of Tables 2 and 3 indicates that this perfect scaling is due to a cancellation of opposite deviations in the case of 10 MeV protons. Table 2 indicates that about 50% of NIEL goes into vacancy formation, which is some 20% more than for the two other radiation types. Table 3, however, shows that for 10 MeV proton irradiation 20% less of vacancies end up in V_2. These two opposite deviations cancel each other and thus re-establish perfect NIEL scaling of $[V_2]$.

Certainly, the simulation models used cannot be claimed to be accurate within 20% but this trend of scaling violation seems quite natural. The non-scaling of the initial vacancy production was discussed before. It was also shown that 10 MeV protons produce more lone vacancies than the other radiation types considered. Thus, it is to be expected that a smaller fraction of these vacancies end up in multi-vacancy defects. This interpretation is supported by the observations that the fraction of vacancies ending up in VO is correspondingly largest for 10 MeV protons and that higher order multi-vacancies become increasingly less probable going from 1 MeV neutrons to 10 MeV protons.

3.2.2. V_3 and V_N formation

The formation of V_3 shows a clear deviation from NIEL scaling. According to Table 3 the fraction of vacancies ending up in higher order multi-vacancies is a factor of 2 lower for 10 MeV protons than for 1 MeV neutrons. This is a clear indication of less cluster contribution in the 10 MeV proton case.

The evolution of higher order multi-vacancies (V_4, V_5 and V_6) is not shown in Fig. 8. The uncertainties of their generation probabilities are significant but under the assumptions made in the simulations the sum of these higher order multi-vacancies is very similar to V_3 in terms of NIEL scaling and about a factor of 4 lower in production rate.

3.2.3. VO formation

The VO defect itself has no significant influence on the electrical properties of the silicon. However, an insight into the evolution of [VO] as a function of fluence is important in order to understand the production of the potentially important, but hypothetical, V_2O defect.

The evolution of [VO], shown in Fig. 8, clearly violates NIEL scaling, which can be understood by the different number of lone vacancies produced by the three irradiation types considered.

[6] The notation [X] is used for concentration of X.

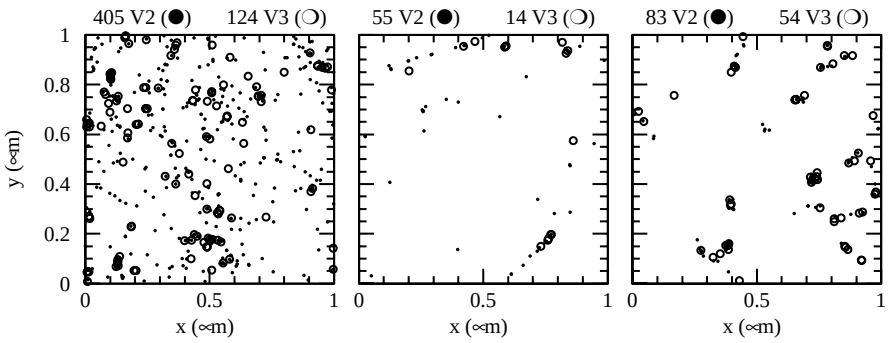

Fig. 7. Final distribution of V_2 (dots) and V_3 (circles) defects after 10 MeV proton (left), 24 GeV/c proton (middle) and 1 MeV neutron (right) irradiation. The plots correspond exactly to the initial vacancy concentration of Fig. 5 and have the same fluence and depth scaling.

Table 3
Fraction of initial vacancies ending up in VO, V_2, V_3 and V_N ($N = 4, 5, 6$) defects for various irradiation conditions. The statistical error is negligible and the dependence on accumulated fluence is small $[O] = 5 \times 10^{15}$ cm^{-3}.

Irradiation type	$[VO]/[V]_{ini}$	$2 \times [V_2]/[V]_{ini}$	$3 \times [V_3]/[V]_{ini}$	$N \times [V_N]/[V]_{ini}$
10 MeV proton	0.0133	0.0191	0.0075	0.0025
24 GeV proton	0.0105	0.0231	0.0119	0.0041
1 MeV neutron	0.0064	0.0227	0.0150	0.0056

3.2.4. V_2O formation

The V_2O defect has been proposed as a possible candidate to explain the changes of N_{eff} and the suppression of V_2O formation has been the main motivation for oxygen enrichment of silicon [24]. This suppression is based on the assumption that vacancies drifting in the silicon will be captured on some impurity—in most cases on O or already formed VO. If the initial [O] is low the [VO]/[O] ratio increases rapidly with fluence and V_2O formation becomes more likely. But if [O] is much higher than the number of introduced vacancies, the [VO]/[O] ratio remains small and most vacancies will be absorbed by oxygen.

This reasoning is perfectly correct if the vacancies are produced uniformly throughout the material, which is the case in, e.g., electron irradiation. However, the clusters formed in hadron irradiation make the issue far more complicated.

The importance of clustering is illustrated in Fig. 8 where three interesting observations can be made:

(1) At low fluences an increase of [O] leads to a higher V_2O production.
(2) With increasing [O] the slope of the V_2O production as a function of fluence becomes shallower.
(3) V_2O production does not scale with NIEL at low [O] but at high [O] it does.

The first of these observations is due to the fact that within a cluster the local V-density is very high and essentially all oxygen inside the cluster will be immediately transformed to VO and subsequently—by vacancies of the same event—many of them to V_2O. In this case, an increase of [O], i.e. more oxygen atoms within a cluster perimeter, leads to an increase of V_2O production at low fluences. Vacancies escaping the cluster fulfil the requirement of uniform distribution and for them an increase of [O] has the desired effect of V_2O suppression.

The second observation is explained by the fact that, at low [O], production of V_2O outside the cluster region dominates and is boosted by the gradual increase of [VO], whereas at high [O] most of the V_2O production takes place within the

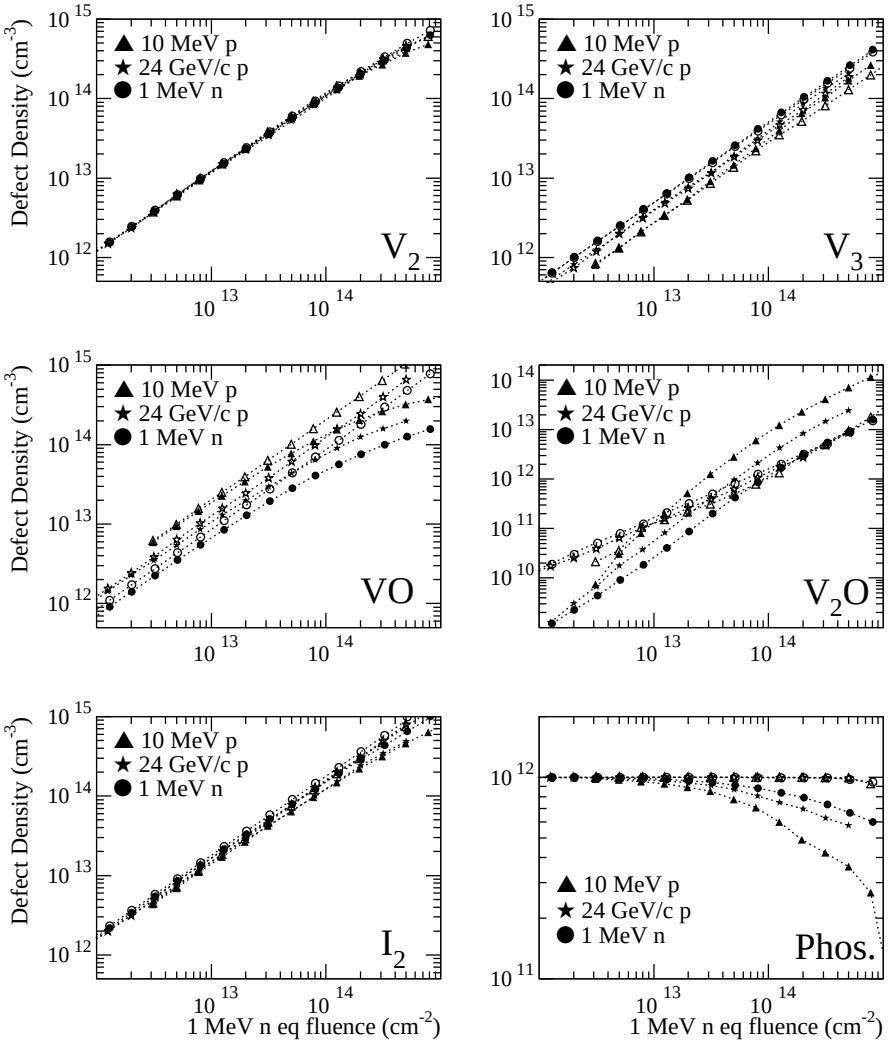

Fig. 8. Concentration of various defects and P-dopant as a function of hadron fluence. Solid symbols correspond to silicon with an initial oxygen concentration of 5×10^{15} cm^{-3}, open symbols to 5×10^{17} cm^{-3}.

cluster and is therefore almost independent of [VO].

The third point is maybe the most interesting one. It is actually a confirmation for the interpretation of the first observation: the production of V_2O outside the clusters, like that of VO, is proportional to the vacancies escaping—or being formed outside—a cluster region and thus should not scale with NIEL. But this formation mode is suppressed at high [O] so that V_2O is formed predominantly inside the clusters. Within the cluster V_2O and V_2 production are essentially the same reaction, except that in the former there is a 'seed' oxygen which first captures a vacancy which then captures another V. Thus, the V_2O production within the cluster should indeed scale with NIEL.

In conclusion, high [O] is suppressing V_2O production only at fluences well beyond 10^{13} cm^{-2}. Since, however, detrimental effects on silicon detectors manifest themselves only in this fluences regime the oxygen addition is likely to be

of advantage. The exception is neutron irradiation, where V_2O production within the cluster appears to dominate at all fluences, independent of [O].

3.2.5. I_2 formation

As explained before the di-interstitial was introduced as a hypothetical defect in order to re-establish consistency of the DLTS data. In this work, no electrical properties are assumed for this defect, so it can be considered as any electrically neutral sink for interstitials. However, the effect of removing interstitials from the system must have secondary implications somewhere. Therefore, it is important to know how many interstitials have been removed. As can be seen, the I_2 formation rate is almost identical to that of V_2. So the I_2—or any other interstitial related defect—has to appear in a quite high concentration in order to make the simulations consistent with the DLTS data.

3.2.6. Phosphorus removal

In the simulations it is assumed that initially $[P] = 10^{12}\ cm^{-3}$ which is much lower than the lowest [O] considered. As a consequence the phosphorus is removed very slowly and, especially for oxygenated silicon, the P-doping remains essentially constant. This slow dopant removal is inconsistent with the exponential 'dopant removal' term which is usually applied to describe experimentally observed changes of N_{eff} at low fluences [37].

However, the present simulation results are fully consistent with observations made in previous simulations [24,37], according to which phosphorus removal is much slower than the exponential decrease of N_{eff}. It also should be pointed out that, according to Table 1, the capture probability of $V + P$ in the simulations is already 20 times higher than that for the competing reaction $V + O$. There is no obvious explanation for this discrepancy between simulations and experiment. One possibility could be that the initial doping concentration is due to strong compensation, i.e. the actual phosphorus concentration is higher than the effective donor concentration. But this is not supported by experimentally measured phosphorus concentrations in detector grade silicon [28]. Such an explanation also would not explain an exponential dependence because already a small fraction of removed phosphorus would lead to intrinsic material, i.e. the decrease should appear essentially linear. The only remaining possibility to explain an exponential donor removal is that the phosphorus is predominantly removed by reactions with a defect, which is not considered in any of the simulations made so far.

Fig. 8 also shows that phosphorus removal is fastest for 10 MeV protons and slowest for 1 MeV neutrons. Again the reason is that in the latter case a larger fraction of the vacancies remain bound to multi-vacancies in the cluster region.

3.3. The "proton–neutron puzzle"

The initial motivation for the present study was to see if a microscopic simulation could cast some light on the rather puzzling experimental observation that oxygenation reduces N_{eff} changes for proton and pion irradiation, but has little effect for neutrons around 1 MeV. Experiments show that in non-oxygenated silicon the N_{eff} changes seem to follow NIEL scaling independent of hadron type or energy, while a higher oxygen content reduces the increase of N_{eff} after type inversion (β-slope) for proton irradiation [38,8,27].

It is immediately clear that if N_{eff} changes would be attributed only to the V_2O defect, Fig. 8 would be in strict contradiction to these experimental findings. According to the preceding discussion, it is quite reasonable that $[V_2O]$ does not follow NIEL-scaling in standard silicon and thus cannot alone explain the observed N_{eff} changes.

It should be reminded at this point that the parameters fitted for the defect migration model have large uncertainties. But, although not reproduced in this paper, several alternative parameter sets were studied and they all reproduced essentially the same $[V_2O]$. This is a clear indication that the model predictions are rather insensitive to the exact choice of the parameters as long as these are in a reasonable range—actually the fit to the DLTS data has a rather shallow minimum with respect to most of the four fitted parameters. Thus, the defect migration model would have to be fundamentally wrong in order to significantly change the prediction for $[V_2O]$. The only defects

which are present in sufficient quantity and which according to the present model—at least roughly—follow NIEL scaling are V_2, V_3 and I_2. The last of these is not claimed to influence electrical properties of silicon.

Omitting the free carriers in the bulk, N_{eff} is the difference between occupied donor and acceptor states. A simple expression for N_{eff}, involving the presumably most important contributors, can be written as

$$N_{\text{eff}} = |[\text{P}] - f_1 \times [\text{V}_2\text{O}] - f_2 \times [\text{V}_2] - f_3 \times [\text{V}_3]| \quad (5)$$

where f_i are constants which express the relative contributions of the defects to the space charge, i.e. the electron occupancies of the acceptor states. Among some others, the defects VP and V_N ($N > 3$) have been omitted. The first because it is produced in minute quantities and the second because its effects are assumed to be overwhelmed by V_2 and V_3.

An inspection of the simulation data for 1 MeV neutrons shows that only V_2 and V_3 appear in sufficient concentrations to induce-type inversion at a fluence of $\sim 10^{13}\,\text{cm}^{-2}$, as observed by experiments before any annealing. But this requires that $f_2 \approx 0.05$ (and/or $f_3 \approx 0.2$) for 1 MeV neutrons.

The values of f_i can be estimated from Shockley–Read–Hall (SRH) theory [39,40] if the defect levels and electron/hole capture cross-sections are known. Under the typical assumption [41] of $\sigma_p = \sigma_n \approx 10^{-15}\,\text{cm}^2$, the values listed in Table 4 are obtained. It should be emphasised that the f_i and I_{leak} values are very sensitive to the energy levels of the defects and the cross-sections assumed. Both have large uncertainties, so any quantitative predictions based on them should be treated with care. As can be seen, the estimated occupancies are far too low to reproduce the experimentally observed type inversion point. Also the leakage current would be severely underestimated. Such a large difference cannot be explained by the uncertainties discussed above. It also seems unlikely that the simulated defect concentrations could be wrong by orders of magnitude because DLTS data for, e.g. V_2 is reproduced. It is possible that DLTS underestimates the V_2 concentrations if the defects are clustered, but it is inconceivable that the clusters could hide 2–3 orders of magnitude more divacancies than are visible by DLTS. According to the simulations there are not even enough primary Frenkel pairs produced to allow for this, even if no I + V recombinations would take place.

Table 4
Defect levels (values in parentheses indicate an assumption), occupancies and contribution to leakage current as calculated from SRH theory assuming $\sigma_p = \sigma_n = 2 \times 10^{-15}\,\text{cm}^2$

Defect type	Energy (eV)	f_i	I_{leak} (μA/defect)
V_2	E_c-0.42	2×10^{-5}	9×10^{-14}
V_3	(E_c-0.47)	7×10^{-4}	6×10^{-13}
V_2O	(E_c-0.55)	0.3	1×10^{-11}

It has been suggested that if defects are clustered their occupancies might be enhanced significantly by the inter-centre charge transfer mechanism [42,43]. Thus f_i for a defect within a cluster might be much higher than for a lone defect of the same type. A detailed calculation [42] has shown that the enhancement for clustered V_2 can reach a factor of 400. Even this does not give a sufficient effect. However, assuming that a similar enhancement exists also for clustered V_3, the simulation results can become consistent with experiment. It is in fact likely that various kinds of defects interact and contribute to their mutual occupation enhancement. Here, only the two lowest order multivacancies will be considered, i.e. V_2 and V_3 are assumed to mutually enhance each others occupancy.[7]

In order to determine the amplification, the density of defects has to be known. This cannot be easily extracted from the simulation results because the clusters have unknown shape and diffuse boundaries. A simple definition has been adopted by considering the local density within a fixed-radius sphere drawn around each defect.

[7] The enhancement is taken from calculation for V_2 clusters [42], which is not exactly correct due to differences in V_2 and V_3 energy levels. But a more detailed calculation is beyond the scope of this paper.

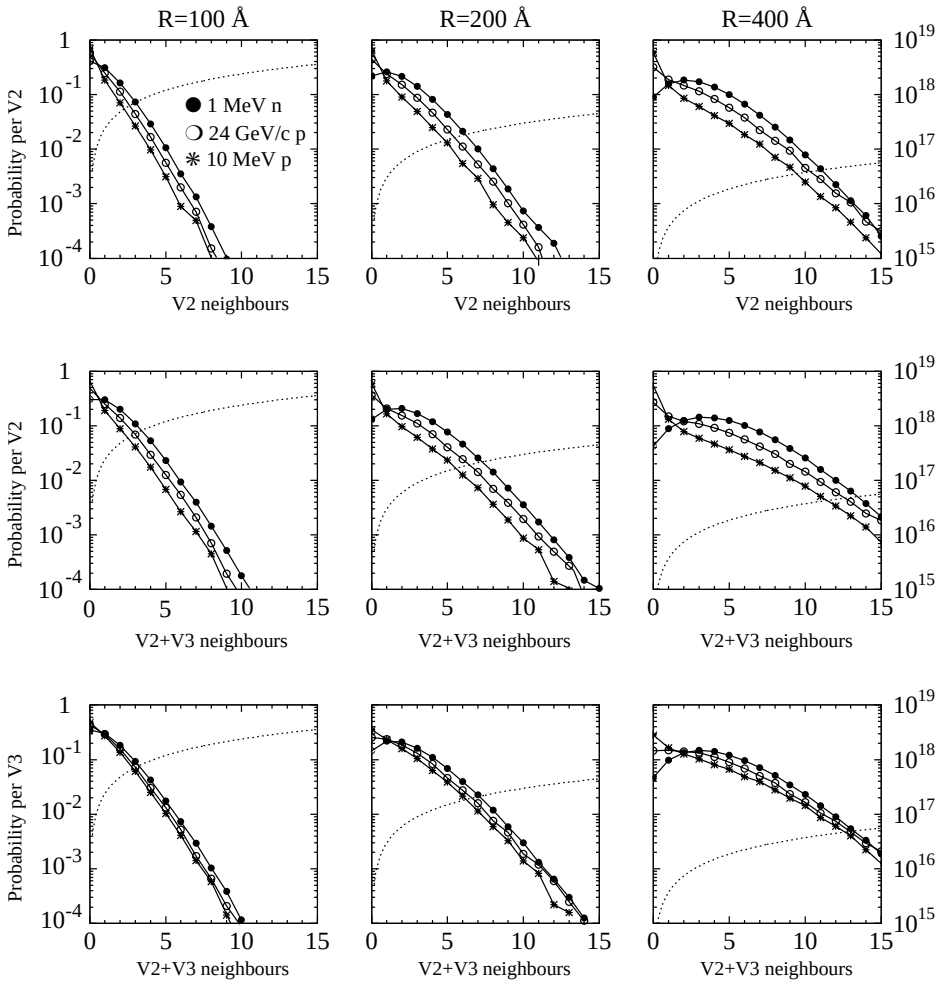

Fig. 9. Probability of finding N neighbours within a given radius around a defect. The dotted line (right scale) gives the corresponding local defect density in cm^{-3}.

Fig. 9 shows the probability distribution of this local density for three different radii of the sphere. The plots indicate that densities of $10^{18}\ \mathrm{cm}^{-3}$—where the enhancement should saturate—can be achieved only in rather small volumes and the contributing number of defects is small. This suggests that the enhancement, even within a cluster region, might vary depending on the local density. In order to extract some quantitative estimate the defect distributions have been analysed assuming the enhancement-density dependence given in Ref. [42]. If the local density is less than $10^{15}\ \mathrm{cm}^{-3}$, the defect is interpreted to be outside the cluster. For clustered defects the average enhancement is calculated. The results are summarised in Table 5.

In order to take the enhancement into account $[V_2]$ and $[V_3]$ must be split into clustered and non-clustered components with different contributions to N_{eff}:

$$N_{\mathrm{eff}} = |[\mathrm{P}] - f_1[\mathrm{V_2O}] - f_2\{E_2 f_c^2 + (1 - f_c^2)\}[\mathrm{V_2}] - f_3\{E_3 f_c^3 + (1 - f_c^3)\}[\mathrm{V_3}]| \quad (6)$$

Table 5
Fraction of clustered defects (f_c^i) and an estimate of their average occupancy enhancement (E_i) for two values of the radius over which the local density is determined

		1 MeV Neutron		24 GeV/c Proton		10 MeV Proton		200 MeVπ^+	
Defect type	R (Å)	f_c^i	E_i	f_c^i	E_i	f_c^i	E_i	f_c^i	E_i
V_2	100	0.70	288	0.51	277	0.35	269	0.56	279
V_3	100	0.65	281	0.57	274	0.51	271	0.59	276
V_2	200	0.87	64	0.64	58	0.41	55	0.70	59
V_3	200	0.85	62	0.74	58	0.64	56	0.77	59

where f_i are the occupancies given in Table 4, f_c^i are the clustered defect fractions and E_i the mean enhancements from Table 5.

At this point it should be emphasised that the simulations reproduce the situation prior to annealing[8] while experimental data is usually obtained after a lengthy annealing period at elevated temperature [8]. According to DLTS data [V_2] does not change during annealing [28]. It is reasonable to assume also [V_2O] to be stable. The V_3 defect, however, has been associated with a DLTS signal that does anneal [25,28].

It turns out that Eq. (6), with the f_i values from Table 4 and the $R = 100$ Å values from Table 5, can be made consistent with experimental observations only if a certain amount of the V_3 defects have annealed. If all the initial V_3 are present, the oxygen concentration has little effect and NIEL scaling is slightly violated. This behaviour is not very serious, because there is no experimental data about the effect of oxygen immediately after irradiation. If all the V_3 are assumed to have disappeared—which might be the case after long annealing—the oxygen effect is large, but NIEL scaling is quite badly violated for non-oxygenated silicon. In this case, protons and pions appear more damaging than 1 MeV neutrons. This contradicts experimental findings for NIEL scaling but it should be remembered that the present model probably does not include all contributing effects and it is well possible that some other defects—possibly related to reverse annealing—start to dominate the N_{eff} or leakage current

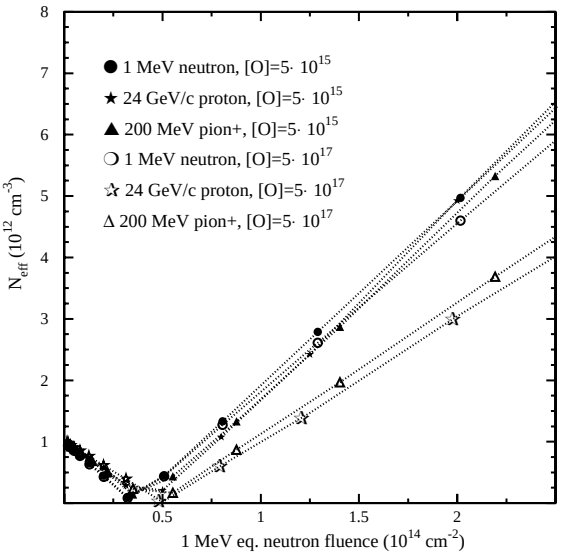

Fig. 10. N_{eff} evolution as a function of fluence, predicted by Eq. (6) for 1 MeV neutrons, 24 GeV/c protons and 200 MeV positive pions. Fluences are scaled with respect to 95 MeV mb using the simulated values of NIEL.

around the time when a significant fraction of the V_3 have annealed. Also the enhancement factors of Table 5—assumed constant in the simulation—are likely to change during annealing. In any case, the model suggests that the effect of oxygen is likely to depend on the annealing state at the time of measurement. With the present assumptions for the model parameters the oxygen effect should get amplified in the course of annealing.

Assuming 30% of the initial [V_3] to be left—which could correspond to a particular annealing state—the N_{eff} evolution shown in Fig. 10 is

[8] The DLTS data used to fit the model corresponds to a situation very shortly after the irradiation.

obtained. At a qualitative level the experimentally observed effects of oxygen enrichment [27] are reproduced by the simulation. But this is achieved only if the V_2O defect has an occupancy close to unity, i.e. is very close to mid-gap and if V_2 and V_3 defects play an important role. In particular, the occupancy enhancement caused by clustering of these defects appears to be mandatory in order to get predictions into the right order of magnitude.

Although the qualitative agreement of Fig. 11 and the data in Ref. [27] is good, the simulated effect of the oxygen for proton irradiations is slightly less pronounced than in the experimental data [27]. But it has been pointed out that there are also significant inconsistencies among experimental data [44]. Eq. (5) includes only the presumably most important defects and inclusion of others might slightly change the picture. In addition the experimental data concern the situation after beneficial annealing whereas the simulations consider only a partial annealing of $[V_3]$—it is certain that many other processes are taking place in irradiated silicon. Thus, it is possible that the oxygen effect is amplified during the annealing. In addition, the simulations assume a uniform oxygen profile, which does not exactly correspond to reality.

Irrespective of these uncertainties the simulations make one rather strong prediction illustrated in Fig. 11: without attempting to make a truly qualitative prediction, the model seems to require that the effect of oxygen should be very pronounced for 10 MeV protons. So far only one group has systematically studied the effects of oxygenation for low-energy protons [45]. The results show a clear but not very pronounced effect. However, there are three important aspects to note: Ref. [45] does not provide a comparison of the same diodes for 24 GeV/c protons, the difference in oxygen concentration of the diodes is 1 order of magnitude compared to 2 orders of magnitude in the simulations and the lowest proton energy is 16 MeV. As shown in Ref. [12] inelastic events, i.e. a higher percentage of clustered defects, become important just between 10 and 20 MeV and therefore the difference between 10 and 16 MeV could be very significant.

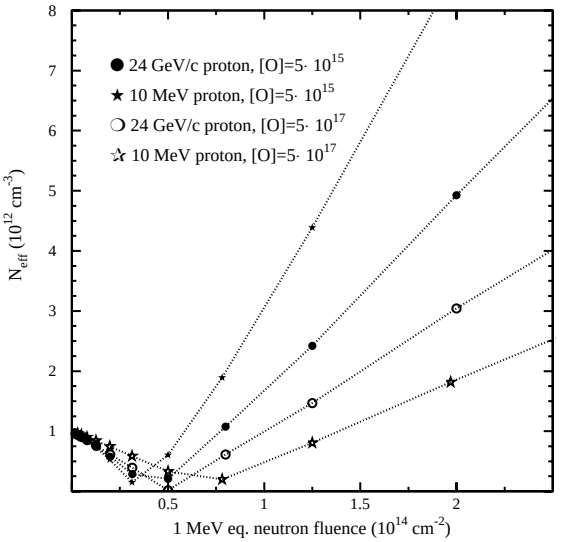

Fig. 11. N_{eff} evolution as a function of fluence, predicted by Eq. (6) for 24 GeV/c and 10 MeV protons. Fluences are scaled with respect to 95 MeV mb using the simulated values of NIEL.

Fig. 11 appears to imply a significant NIEL violation for standard silicon but the plot has been scaled with the hardness factor[9] of 3.1 simulated in this work, which is lower than the usual assumption [1]. It has been recently measured that β for 10 MeV protons scales with NIEL if a hardness factor of about 4 is assumed [32]. If a hardness of 4–4.5 would be used in Fig. 11 then an apparent NIEL scaling would be restored for standard silicon, i.e. the 10 MeV and 24 GeV/c curves would roughly overlap.

4. Consequences for leakage current

The leakage current can be estimated using the values given in Table 4 and the simulated defect concentrations. However, also the effects of the clustering and the resulting enhancements have to be taken into account. As a first approximation one can assume that the enhancement of leakage current is proportional to the enhancement of the occupancies f_i.

[9] NIEL relative to 95 MeV mb.

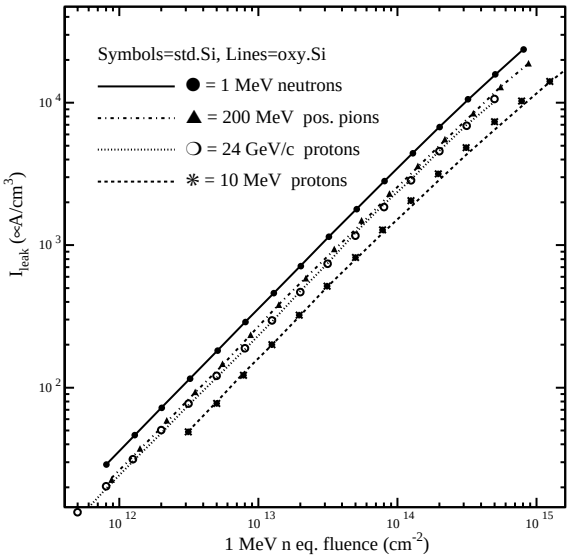

Fig. 12. Leakage current as a function of fluence for various irradiation types. Fluences are scaled with respect to 95 MeV mb using the simulated values of NIEL.

In the preceding section a possible explanation for the proton–neutron puzzle of N_{eff} was presented, but it appears that the solution introduces a new discrepancy, shown in Fig. 12: the NIEL scaling of the leakage current constant (α) is quite severely violated. Since the NIEL scaling of α is generally considered to be a well established experimental fact, this appears to be a shortcoming of the model and could mean that some component is not properly accounted for.

The values of α, extracted from the simulations, are in a reasonable range $1.7\text{–}3.7 \times 10^{-17}$ A/cm for the same condition as in Fig. 10, i.e. 70% of the V_3 annealed.

Considering that Fig. 8 indicates perfect NIEL scaling for the [V_2] and assuming that the V_2 defect is the dominant contributor to α, a NIEL violation, as indicated in Fig. 12, necessarily arises from the enhancement caused by the V_2-clustering.

On the other hand, this clustering is required also to get a reasonable value for α. Thus, there seems to be at the same time verification and contradiction for the assumption of enhancement in the clusters. In Fig. 12 the simulated hardness factor of 3.1 has been used for 10 MeV protons, but 1.5 would be needed to make α agree with that for 1 MeV neutrons. Thus, the deviation from NIEL scaling is in the other direction than for N_{eff}.

It is beyond the scope of this work to elaborate on the model of the enhancement mechanism within the cluster. It has been shown, however, that the enhancement is very sensitive to the defect energy levels and capture cross-sections [46]. In addition, the enhancement of α is not necessarily the same as that of the f_i-values. If many defects contribute to the cluster—which is almost certain to be the case—a calculation of the enhancement can become very complicated. One possibility could be that the cluster size plays a role and in a larger cluster, typical for 1 MeV neutrons, transitions between various defect levels compete with transitions to the conduction band and thus quench the leakage current enhancement without affecting the average occupancies. However, it would be surprising if such complicated mechanisms would be needed to compensate for each other in order to maintain NIEL scaling of α at all stages of annealing.

It is also possible that the result of Fig. 12 is not so wrong after all. An experimental determination of α for 1 MeV neutron is very problematic due to the rapidly oscillating damage function shown in Fig. 3. A more reliable NIEL comparison can be obtained by comparing 10 MeV protons with 24 GeV/c protons.

Indeed, recent experiments give a ratio of only 4 for α of 10 MeV and 24 GeV/c protons [32]. The corresponding ratio extracted from Fig. 12—taking account of the already performed NIEL scaling according to Table 2—is 4.5. This corresponds to a hardness factor of 2.5 for α—significantly different from the 4–4.5 found for β.

Thus, the simulations seem to be almost perfectly consistent with recent N_{eff} and leakage current measurements comparing 10 MeV and 24 GeV/c protons. But this means that NIEL scaling is, indeed, significantly violated in both cases—and even in opposite directions.

For hadron irradiations clustered V_2 seem to always dominate the leakage current. Thus, the oxygen concentration has no effect. This situation, however, should be different for electron irradiation where essentially no clusters are formed. In this case the V_2O defect should gain on importance

and consequently the α-constant should be decreased at high [O].

5. Conclusions

A fully microscopic simulation of NIEL in silicon is presented. It is shown that the results are rather consistent with previously quoted NIEL values, but some non-negligible deviations can be observed. These highlight the uncertainties in any 'theoretical' calculation of NIEL.

It is furthermore shown that the ratio between produced vacancies and simulated NIEL can vary by 20%, depending on hadron type and energy, but in general the number of produced vacancies follows well the modified Kinchin–Pease relation.

A defect kinetics model is developed based on the ideas of Ref. [21], but complemented with a random-walker model to account for variations of defect densities within cluster regions. Parameters required by this model are taken from Ref. [24] when available and otherwise extracted by fitting the simulations to DLTS data of neutron irradiated silicon. The model is then used to predict densities of complex defects, V_2, V_3, VO, V_2O, etc. in silicon irradiated with various types of hadrons.

The model shows that only V_2 concentrations are proportional to the simulated NIEL for all three irradiation types considered. Even this is due to the fact that a 20% NIEL-violation in formed vacancies is compensated by an opposite 20% effect due to different vacancy–vacancy correlations. Production of all other defect types considered shows a more or less significant violation of NIEL scaling.

It is shown—fully consistent with Ref. [47]—that if standard Shockley–Read–Hall theory is used, the concentrations of the defects are not sufficiently high to explain observed electrical properties of hadron irradiated silicon. If an enhancement of defect occupancy due to clustering of defects is introduced, the experimentally observed changes of N_{eff} and leakage current can be reproduced. There are many uncertain parameters in the model which make a truly quantitative prediction impossible, but on a qualitative level the model can reproduce the observed effect that oxygen enrichment reduces the β-slope of N_{eff} for proton and pion irradiation whereas it has little effect in the case of 1 MeV neutrons.

Almost irrespective of the assumptions made (unless the V_2O defect is assumed to be essentially inactive) the model predicts that oxygen enrichment should have a very pronounced effect in the case of 10 MeV proton irradiation. This should provide a good test for the model and/or the role of the V_2O defect—but due to the significant uncertainties of the input parameters, only at a qualitative level.

The simulation model makes the quite unorthodox prediction that NIEL scaling should be violated both for the leakage current constant α and the β-slope of the effective doping concentration after type inversion. The violation is predicted to be in opposite directions and most pronounced in the case of low-energy protons.

While there are uncertainties in the model, which could be argued to be the cause of such a prediction, recent experimental data on 10 MeV protons seems to agree very well with the simulations, thus strengthening the case for the existence of such NIEL violations. In any case it should be emphasised—with reference to Fig. 3—that an experimental value for the hardness of a typical (reactor) neutron spectrum is very difficult to obtain. Thus, a NIEL scaling with respect to neutrons is likely to introduce non-negligible experimental errors, which can mask quite substantial NIEL violations. Also for other hadrons the 'theoretical' NIEL predictions are shown to have significant uncertainties. Much of the reported work on NIEL scaling is actually comparison of Si-damage data to other Si-damage data. A direct experimental measurement of NIEL itself does not exist. Against this background the validity of NIEL scaling might not really be as firmly established as is usually believed.

Acknowledgements

The people who have provided advice and suggestions are too numerous to be all listed here. Of particular importance was the suggestion of Dr. K. Saarinen (Helsinki University of Technology)

to use a simple random walk model for defect migration. Special thanks go to Dr. K. Gill and Dr. M. Moll (both CERN) who have patiently answered my numerous questions and also made valuable comments to the final paper.

References

[1] A. Vasilescu, G. Lindström, CERN ROSE/TN/2000-02, 2000.
[2] G. Simon, J. Denney, R. Downing, Phys. Rev. 129 (1962) 2454.
[3] E. Burke, IEEE Trans. Nucl. Sci. NS-33 (6) (1986) 1276.
[4] G. Summers, et al., IEEE Trans. Nucl. Sci. NS-34 (6) (1987) 1134.
[5] V. Van Lint, Nucl. Instr. and Meth. A 253 (1987) 453.
[6] C. Dale, et al., IEEE Trans. Nucl. Sci. NS-35 (6) (1988) 1208.
[7] A. Van Ginneken, Fermilab Note FN-522, 1989.
[8] G. Lindström, et al., Nucl. Instr. and Meth. A 465 (2001) 60.
[9] M. Huhtinen, P.A. Aarnio, Nucl. Instr. and Meth. A 335 (1993) 580.
[10] P.A. Aarnio, et al., Nucl. Instr. and Meth. A 360 (1995) 521.
[11] S. Bates, et al., Nucl. Instr. and Meth. A 379 (1996) 116.
[12] M. Huhtinen, F. Faccio, Nucl. Instr. and Meth. A 450 (2000) 155.
[13] A. Fassò, A. Ferrari, J. Ranft, P. Sala, Specialists' Meeting on Shielding Aspects of Accelerators, Targets and Irradiation Facilities, Arlington, Texas, April 28–29, 1994 NEA/OECD doc. 1995, p. 287.
[14] A. Fassò, A. Ferrari, J. Ranft, P. Sala, in: A. Menzione, A. Scribano (Eds.), Proceedings of the IV International Conference on Calorimetry in High Energy Physics, La Biodola, September 20–25, 1993, World Scientific, Singapore, 1993, p. 493.
[15] K. Hänssgen, J. Ranft, Comput. Phys. Commun. 39 (1986) 53.
[16] M. Huhtinen, Highly ionising events in silicon detectors, CERN CMS NOTE-2002/011, 2002.
[17] I. Tomalin, Presentation at the CMS General Tracker Meeting, CERN, 25 January 2002, unpublished.
[18] R.J. Glauber, G. Matthiae, Nucl. Phys. B 21 (1970) 135.
[19] M. Huhtinen, P. Aarnio, HU-SEFT-R-1993-02, 1993.
[20] J.F. Ziegler, J.P. Biersack, U. Littmark, The Stopping and Range of Ions in Solids, Vol. 1, Pergamon Press, New York, 1985.
[21] G. Davies, et al., Semicond. Sci. Technol. 2 (1987) 524.
[22] G. Oehrlein, et al., J. Appl. Phys. 54 (1983) 179.
[23] Y. Shi, et al., J. Appl. Phys. 67 (1990) 1116.
[24] B. MacEvoy, G. Hall, K. Gill, Nucl. Instr. and Meth. A 374 (1996) 12.
[25] M. Ahmed, et al., Nucl. Instr. and Meth. A 457 (2001) 588.
[26] A. Bongiorno, L. Colombo, Phys. Rev. B 57 (1998) 8767.
[27] The ROSE Collaboration, 3rd RD48 Status Report, CERN/LHCC 2000-009, 2000.
[28] M. Moll, Ph.D. thesis, DESY-THESIS-1999-040, 1999.
[29] S. Watts, Brunel University, private communication.
[30] J.L. Hastings, S.K. Estreicher, P.A. Fedders, Phys. Rev. B 56 (1997-II) 10215.
[31] G. Summers, et al., IEEE Trans. Nucl. Sci. NS-40 (1993) 1372.
[32] D. Bechevet, et al., Nucl. Instr. and Meth. A 479 (2002) 487.
[33] P.J. Griffin, et al., SNL RML Recommended Dosimetry Cross Section Compendium, Sandia National Laboratories, SAND92-0094, 1993.
[34] A. Konobeyev, et al., J. Nucl. Mater. 186 (1992) 117.
[35] ASTM Annual Book of Standards, Vol. 12.02, 1985, p. 323.
[36] A.I. Namenson, E.A. Wolicki, G.C. Messenger, IEEE Trans. Nucl. Sci NS-29 (1982) 1018.
[37] M. Moll, E. Fretwurst, G. Lindström, Nucl. Instr. and Meth. A 439 (2000) 282.
[38] A. Ruzin, Nucl. Instr. and Meth. A 447 (2000) 116.
[39] W. Shockley, W.T. Read, Phys. Rev. 87 (1952) 835.
[40] R. Hall, Phys. Rev. 87 (1952) 387.
[41] S. Sze, Semiconductor Devices, Physics and Technology, Wiley, New York, 1985.
[42] K. Gill, G. Hall, B. MacEvoy, J. Appl. Phys. 82 (1997) 126.
[43] S.J. Watts, et al., IEEE Trans. Nucl. Sci. 43 (6) (1996) 2587.
[44] M. Moll, CERN, private communication.
[45] J. Wyss, et al., Nucl. Instr. and Meth. A 457 (2001) 595.
[46] K. Gill, CERN kindly repeated some calculations of Ref. [42] with various speculative assumptions to study the sensitivity.
[47] B. MacEvoy, Nucl. Instr. and Meth. A 388 (1997) 365.